Macromolecules

Article

pubs.acs.org/Macromolecules

Structure and Dynamics of Polyelectrolyte Complex Coacervates Studied by Scattering of Neutrons, X-rays, and Light

Evan Spruijt,[†] Frans A. M. Leermakers,[†] Remco Fokkink,[†] Ralf Schweins,[‡] Ad A. van Well,[¶] Martien A. Cohen Stuart,[†] and Jasper van der Gucht*[,†]

[†]Laboratory of Physical Chemistry and Colloid Science, Wageningen University, Dreijenplein 6, 6703 HB Wageningen, The Netherlands

[‡]DS/LSS Group, Institute Laue-Langevin, 6 Rue Jules Horowitz, F-38042 Grenoble Cedex 9, France, and

[¶]Department of Radiation Science and Technology, Delft University of Technology, Mekelweg 15, 2629 JB Delft, The Netherlands

Supporting Information

ABSTRACT: We investigate the microscopic structure and density fluctuations of complex coacervates of flexible polyelectrolytes using scattering of neutrons, X-rays, and light. Poly(acrylic acid) and poly(*N*,*N*-dimethylaminoethyl methacrylate) offer a well-defined model system that allows for selective labeling and systematic variation of the strength of the attractive electrostatic interactions. Two neutron scattering experiments have been carried out: (i) we use deuterated polymeric tracers in a complex coacervate with an overall neutron scattering length density that is matched to that of the solvent, to probe the conformation of single polymer chains in the complex coacervates, and (ii) we measure complex coacervates in which all polymer chains of one type are deuterated, to probe their overall structure. The single chain static structure factors reveal that both polycations and polyanions have an ideal Gaussian chain conformation in the complex coacervates. At the same time, the overall structure is similar to that of a semidilute polymer solution, with polycations and polyanions strongly overlapping to form a network with a mesh size that is much smaller than the radius of gyration of the polymers. The mesh size decreases with decreasing salt concentration, following a scaling that is in good agreement with predictions from the corresponding salt−polymer phase diagram. These findings are confirmed by complementary X-ray scattering experiments. Finally, in all scattering experiments with light, X-rays, and neutrons, and for all polymer chain lengths and salt concentrations, we find a remarkable low-*q* excess scattering, following a power law with a slope close to −2. This points to the presence of equilibrium, large-scale density fluctuations in the complex coacervates. Dynamic light scattering experiments reveal two complementary diffusive modes in the complex coacervates, corresponding to fluctuations of the polymer mesh and diffusion of domains of varying density, respectively.

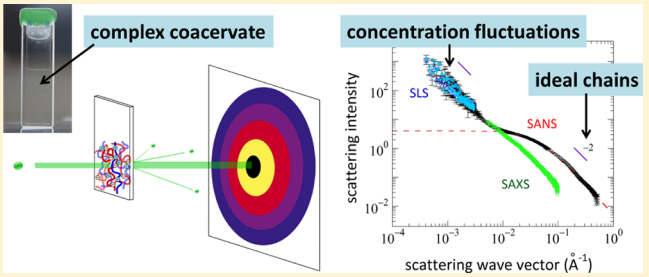

INTRODUCTION

Complex coacervates are dense phases of oppositely charged macroions, which typically contain large amounts of hydration water.[1,2] They form by associative phase separation of a mixture of the oppositely charged species and are essentially liquids.[3−6] Complex coacervates and the underlying process of coassembly of oppositely charged species are ubiquitous in natural and man-made materials. The underwater glue of the sandcastle worm,[7] the bacterial nucleoid,[8,9] and chromatin fibers of DNA-histon complexes[10−12] are but a few examples of such natural electrostatic assemblies. In man-made materials, nature's approaches are often mimicked to create, for example, membranes,[13] vesicles,[14] spherical and wormlike micelles,[15] fibers,[16] and soft gels.[17]

The combination of strong intermolecular associations and strong hydration provides a delicate balance that is expected give rise to interesting assemblies.[1] Fine-tuning of these structures to meet the needs for their application as new coatings, drug carriers or bioadhesives requires detailed knowledge about the structure of complex coacervates and the underlying driving forces. Many dynamic and mechanical properties of complex coacervates are closely related to their structure.[5] However, little is known about the microscopic structure of complex coacervates.

Hone et al. were the first to use small-angle neutron scattering (SANS) to study the structure of complexed, but not phase separated, polyelectrolytes in solution.[18] They found that the addition of small amounts of poly(styrenesulfonate) or poly(2-acrylamido-2-methylpropanesulfonate) to α-gelatin solutions above the melting temperature gave rise to a strong increase in solution viscosity due to complexation. The structure factors displayed a peak that is similar in shape and

Received: January 19, 2013
Revised: May 17, 2013
Published: May 31, 2013

   dx.doi.org/10.1021/ma400132s | *Macromolecules* 2013, 46, 4596−4605

Table 1. Specifications of the PDMAEMA and PAA Used in This Study on the Structure of Polyelectrolyte Complex Coacervates[a]

polymer	M_n (kg/mol)	M_W (kg/mol)	M_W/M_n	N	ρ (kg/m^3)	ρ_N (10^{-6} Å^{-2})
h-PDMAEMA$_{156}$	23.5	24.4	1.04	156	0.934[b]	0.80[27]
h-PDMAEMA$_{574}$	82.7	90.1	1.09	574		
d-PDMAEMA$_{154}$	25.5	26.5	1.04	154	1.023[c,d]	6.23
d-PDMAEMA$_{800}$	55.0	137.5	2.5	800		
h-PAA$_{160}$	10.0	11.5	1.15	160	1.051[28]	1.46[29]
h-PAA$_{550}$	36.0	39.6	1.10	550		
d-PAA$_{514}$	8.0	38.4	4.8	514	1.095[c]	5.05[30]

[a]N is the weight-averaged degree of polymerization, calculated from M_w, ρ is the bulk density of the polymers, and ρ_N is the coherent neutron scattering length density. All polymers were purchased from Polymer Source. PAA refers to the acidic form (H or D, respectively) of poly(acrylic acid) and PDMAEMA refers to the free amine form of poly(*N*,*N*-dimethylaminoethyl methacrylate). Note that the scattering length density of the respective salts (K and Cl) of both polymers will differ from the values above (see Supporting Information). [b]Assumed to be equal to the density of the liquid monomer. [c]Assuming equal molecular volumes v_m, compared to hydrogenated polymers and correcting for the increase in mass due to deuterium. [d]If the density of d-PDMAEMA is taken the same as the density of h-PDMAEMA, ρ_N would be 5.7.[31]

position to the peak of a solution of only PSS or PAMPS polyelectrolytes, but enhanced in intensity by the strongly associated gelatin molecules. In this case, the long synthetic polyelectrolytes seem to dictate the structure of the complexes, and the complexation with the shorter gelatin gives rise to the enhanced viscosity. Application of shear flow to these viscous solutions leads to anisotropy in the scattering intensity, due to alignment of the polyelectrolyte chains, but not to changes in the complexation behavior.[19] Unfortunately, the structural investigation was only carried out at a single mixing ratio of polyelectrolytes and gelatin. Whether the structure would change when a complex coacervate is formed from these macroions, in which the polyelectrolytes are, inevitably, also close together in a dense liquid-like phase, remains unclear.

Weinbreck et al. used fluorescence recovery after photobleaching (FRAP), nuclear magnetic resonance (NMR), and diffusive wave spectroscopy (DWS) to obtain information on the structure of whey protein/gum arabic complex coacervates.[20] They found that both components in the complex coacervate had reduced diffusion coefficients compared to dilute solutions, but could not probe length scales smaller than roughly 1 μm. In the case of NMR and DWS, a sample-averaged diffusion coefficient was measured. Similar to the findings of Hone et al., one of the components had a much lower diffusivity. In this case, the gum arabic dictates the complex coacervate structure and is less mobile, whereas the whey protein is associated with this structure, but much more mobile. More importantly, these findings show that both components diffuse independently through the complex coacervate.

Kayitmazer et al. discussed the structure of another protein-containing complex coacervate, PDADMAC/BSA, based on light scattering, cryo-transmission electron microscopy (cryo-TEM), FRAP, SANS, and rheology measurements.[21] From rheology and SANS it was found that again the long polyelectrolyte, PDADMAC, dictates the overall network structure of these complex coacervates, and BSA associates with this structure.[6,22] This proposed microstructure is very similar to the microstructure that was found by Wang et al. for β-lactoglobulin/pectin complex coacervates.[23] Complementary to the SANS measurements, dynamic light scattering (DLS), FRAP, cryo-TEM, and NMR measurements were carried out on the PDADMAC/BSA complex coacervates.[21] These measurements all indicated the existence of domains of varying density that were much larger than the correlation length of the semidilute PDADMAC polyelectrolyte network inside the complex coacervates. Dense domains with high concentrations of BSA, complexed with the PDADMAC network, are thought to coexist with more dilute domains with a lower concentration of BSA, which is also more loosely associated with the PDADMAC. The slow and fast diffusive modes that were measured in DLS, FRAP, and NMR thus correspond to BSA diffusion in these respective domains. A power law scaling at low q in SANS and in static light scattering (SLS) agrees with an expected size distribution of the domains of 300−700 nm. Finally, dense domains could be directly observed by cryo-TEM.[21] Similar dense domains have been observed in complex coacervates of lysozyme/PSS, chitosan/BSA, and PDADMAC/SDS.[6] At this point, it remains unclear how such mesoscale heterogeneity in protein−polyelectrolyte and micelle−polyelectrolyte complex coacervates can be explained.

Singh et al. studied the structure of agar/gelatin complex coacervates by means of SANS and differential scanning calorimetry.[24] Both biopolymers form gels separately and the complex coacervates retain the thermal properties of the constituents to a remarkable extent. The authors believe the complex coacervates are physically entangled, interpenetrating networks of the two biopolymers, with mesh size of 1.2 nm. Interestingly, they found excess scattering in the low q regime of their SANS measurements, similar to Kizilay et al.,[6] which they attribute to large-scale concentration fluctuations, with a typical correlation size of 22 nm, even though no leveling off of the intensity was observed.

Chodankar et al. studied the structure of PSS/BSA complex coacervates at low pH by SANS.[25] They found very similar scattering curves as Singh et al. and Kizilay et al., characterized by a mesh size at high q and large-scale density correlations, following a power law scaling, resembling a fractal aggregate. They also measured the scattering intensity from a sample of the dilute phase and found that aggregates with a typical size of several PSS chains were present there. Unfortunately, no explanation was given for the origin of fractal-like structures and power law scaling of the scattering intensity in complex coacervates.

Summarizing the above, the structure of most complex coacervates is far from understood. In protein−polyelectrolyte and micelle-polyelectrolyte complex coacervates, the longer polyelectrolyte molecules seem to dictate the overall structure of the complex coacervate networks and proteins are associated with this network. These associations appear to be heteroge-

neous on mesoscopic length scales between tens of nanometers and a micrometer, giving rise to fluctuations in concentration and excess scattering at low q, in all cases following an apparent power law with a slope of -2 ± 0.5.

When complex coacervates consist of two flexible polyelectrolytes of almost equal length, the microscopic structure is unknown so far. Several intriguing questions arise. Will only one of the components dictate the overall network structure? Will the strong associations between the flexible polyelectrolytes lead to strong pairing into stiff bundles ("ladder" model) or will the complex coacervate behave as an interpenetrating semidilute solution? Will the oppositely charged polyelectrolytes diffuse independently and, finally, will the concentration fluctuations persist?

In this paper, we use scattering of neutrons, X-rays, and light to study the static structure of complex coacervates of flexible polyelectrolytes. We use deuterated polyelectrolytes in complex coacervates with varying neutron scattering length densities to measure the conformation of both flexible polyelectrolytes independently. In addition, we use both polyelectrolytes to determine the structure factor of the complex coacervate networks. We compare our neutron scattering measurements with X-ray scattering and static light scattering measurements, which provide complementary structural information. Finally, from dynamic light scattering we find two modes of relaxation, which we correlate to two types of structural relaxations in the complex coacervates.

MATERIALS AND METHODS

Materials. We prepared complex coacervates from poly(acrylic acid) (PAA), a polyanion with pH-dependent charges, and poly(*N*,*N*-dimethylaminoethyl methacrylate) (PDMAEMA), a polycation with pH-dependent charges. We used fully hydrogenated and fully deuterated versions of both polymers, with specifications as shown in Table 1.

We prepared stock solutions of all polymers at 50 g/L (PDMAEMA) or 30 g/L (PAA) in Milli-Q water with the pH adjusted to 6.5 ± 0.2 using 1.0 M HCl and KOH. The meter readings in solutions containing D_2O were corrected for the difference between pH and pD measured by a glass electrode, using $pK_w = 14.8$ of D_2O.[26] At pH = 6.5, the two oppositely charged polyelectrolytes have equal charge densities for all salt concentrations we used.[4]

For the preparation of the complex coacervates, we used stock solutions of 3.0 M KCl, 1.0 M HCl/DCl, and KOH/KOD in Milli-Q water (resistance >18.2 MΩ·cm) and in D_2O (99.9% D, Sigma-Aldrich), respectively. Before mixing, all stock solutions were filtered using 0.2 μm polyethersulfone membrane syringe filters for H_2O, D_2O, and 3.0 M KCl and cellulose filters (Whatman, grade 1) for the polymer solutions.

The complex coacervate samples were prepared in plastic vials by mixing the PDMAEMA and PAA at the preferred complex coacervate composition, that is, in a 1:1 molar ratio of chargeable groups at an overall concentration of monomeric groups of 0.20 M.[4] After mixing, the samples were left for 2 days, centrifuged at 3000*g*, and then left for another 2 days for equilibration. The relaxation spectrum of these complex coacervates was recently determined experimentally.[32] The longest relaxation time related to polymer reorganization depends on salt concentration, but it does not exceed 10 min for the salt concentrations we used. Finally, the complex coacervates remain stable for months.

After equilibration the phases were separated and 0.2 or 0.4 mL of the complex coacervate phase was transferred together with 0.1 or 0.2 mL of the dilute phase into 1 mm and 2 mm Hellma quartz cuvettes (see Figure 1) or 2 mm Hilgenberg quartz capillaries. The cuvettes were sealed with fitting Teflon stoppers and a two-component silicon rubber and stored at room temperature until we measured them. For light scattering measurements, we transferred 1.5 mL of complex coacervate phase together with 2.0 mL of dilute phase to a Hellma cylindrical quartz cell of 25 mm outer diameter.

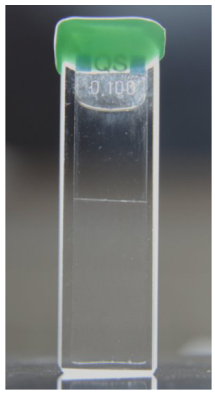

Figure 1. h-PDMAEMA$_{574}$/h-PAA$_{550}$ complex coacervate and coexisting dilute phase in a 1 mm quartz cuvette.

Small Angle Neutron Scattering. Small-angle neutron scattering (SANS) experiments were performed at the Institut Laue-Langevin (ILL) in Grenoble, France, at the D11 beamline. We measured at three detector distances of 1.2, 8.0, and 34.0 m, using collimator distances of 5.5, 8.0, and 34.0 m, respectively. Two incident neutron wavelengths were selected (6 and 13 Å, with a resolution $\Delta\lambda/\lambda$ of 9%), to cover a total q-range of $9.8 \times 10^{-4} < q < 5.2 \times 10^{-1}$ Å^{-1}. We used a sample aperture of 7 × 10 mm^2, and we corrected our data for background scattering, detector response, and intensity fluctuations of the incident beam. We radially averaged our data and converted to absolute scattering cross sections in cm^{-1} using water as a secondary calibration standard, cross-calibrated to well-characterized polymer standards, according to standard ILL procedures. The temperature was kept constant at 18 ± 0.5 °C, unless stated otherwise, to make the measurement temperature identical to the temperature at which the samples were originally prepared.

We carried out SANS measurements for two types of samples. First, we prepared complex coacervates from stock solutions of hydrogenated polymers, to which trace amounts (3.3% or 10%) of either of the deuterated polymers were added, at different salt concentrations, to investigate the conformation of individual polymers in the complex coacervates. For these measurements we used a H_2O/D_2O mixture as a solvent, with volume fraction of H_2O $\phi_w = 0.73$, and consequently, a volume fraction of D_2O $\phi_d = 0.27$. At this solvent composition the average scattering length density of the complex coacervates is matched to that of the solvent. We verified this match point experimentally by measuring the neutron scattering intensity for five PDMAEMA$_{574}$/PAA$_{550}$ complex coacervates at $c_s = 1.1$ M at $\phi_w = 0.65$, 0.70, 0.75, 0.80, and 0.85. We found a minimum scattering intensity at an interpolated $\phi_w = 0.73$ for $5 \times 10^{-3} < q < 2 \times 10^{-2}$ Å^{-1} (see Supporting Information). The scattering intensity is not absolutely zero after solvent correction, but a small offset remains at high q, probably because we cannot match the solvent to the scattering length density of both PAA and PDMAEMA, which have different scattering length densities, at the same time. We subtracted this offset from all our scattering curves, to correct for this effect of scattering length density difference. The second type of samples we prepared were samples in which all polymers of one type were deuterated and the scattering length density of the solvent was matched to that of the other polymer ($\phi_w = 0.81$ for d-PAA/h-PDMAEMA and 0.62 for h-PAA/d-PDMAEMA; the latter value is slightly aberrant because of a miscalculation[29]). All samples were measured in flat Hellma quartz cuvettes with a path length of 2 mm for samples with $\phi_w < 0.65$ and a path length of 1 mm for all other samples.

The SANS scattering curves were fitted using Sasfit.[33]

Small Angle X-ray Scattering. SAXS experiments were performed at the European Synchrotron Radiation Facility (ESRF) in Grenoble, France, at the Dutch–Belgian Beamline (BM26B,

DUBBLE). We used an X-ray energy of 10 keV and a single detector distance of 7.0 m, to cover a total q-range of $6.0 \times 10^{-3} < q < 1.0 \times 10^{-1}$ Å^{-1}. We corrected our data for background scattering, detector response and primary beam intensity fluctuations. We calibrated the instrument scattering vector using a standard specimen of wet rat tail tendon collagen and we converted our data to absolute scattering cross sections using water and HDPE as secondary standards, according to standard ESRF procedures.[34]

We loaded our samples into 2 mm quartz capillaries (Hilgenberg) using syringes and needles and we placed the capillaries into a homemade multicapillary holder. All SAXS measurements were carried out at a temperature of 20 ± 1 °C, the same temperature at which the samples were prepared.

Light Scattering. Dynamic and static light scattering measurements were performed on an ALV light scattering instrument, equipped with a 300 mW Cobolt-Samda DPSS laser, operated at a wavelength of 532 nm, an ALV/SO single photon detector with static and dynamic enhancer fiber-optical technology and an ALV-5000/60X0 external correlator. The temperature was kept constant at 20 ± 0.2 °C using a Haake F8−C35 thermostat. For static light scattering (SLS) measurements, the detector angle was varied from $\theta = 15°$ to $\theta = 141°$ in steps of 2°, to cover a total q-range of $4.1 \times 10^{-4} < q < 3.0 \times 10^{-3}$ Å^{-1}. We converted our data to absolute scattering cross sections in cm^{-1} using toluene as a reference ($R_t = 2.10 \times 10^{-5}$ cm^{-1} at $\lambda = 532$ nm).[35,36] At every detector angle we recorded the scattering intensity in ten runs of 30 s. We corrected the data by subtraction of the solvent scattering, and we report the average corrected values here. For dynamic light scattering (DLS) measurements, the detector angle was varied from $\theta = 20°$ to $\theta = 140°$ in steps of 2°. For every angle we recorded the intensity correlation function $g_2(t)$ and the total scattering intensity I in two subsequent runs, with a total duration per run that increased from 10^2 seconds at $\theta = 140°$ up to 10^4 seconds at $\theta = 20°$.

RESULTS AND DISCUSSION

Small Angle Neutron Scattering. *Conformation of Single Chains in Complex Coacervates.* The phase behavior of complex coacervates of PAA and PDMAEMA depends on both salt concentration and chain length, since the complex coacervates are formed as one of the phases at binodal composition in the associative phase separation of solutions of oppositely charged polymers.[4] The polymer volume fraction inside the complexes varies roughly between 0.05 and 0.30, whereas the overlap concentration varies between $c_p = 0.01$ and 0.1 M, depending on the chain length ($N = 1728-20$, assuming random walk statistics).

We carried out small angle neutron scattering (SANS) experiments on such PDMAEMA/PAA complex coacervates with trace amounts of deuterated PDMAEMA or PAA chains, to determine the conformation of individual polymer chains in complex coacervates. We prepared complex coacervates with trace amounts of d-PDMAEMA$_{154}$ in complex coacervates of h-PDMAEMA$_{156}$/h-PAA$_{160}$ and complex coacervates with trace amounts of either d-PDMAEMA$_{800}$ or d-PAA$_{514}$ in complex coacervates of h-PDMAEMA$_{574}$/h-PAA$_{550}$. The short d-PDMAEMA$_{154}$ and the hydrogenated chains surrounding them in the complex coacervate all have a narrow size distribution and almost equal chain lengths. The longer d-PDMAEMA$_{800}$ and d-PAA$_{514}$ have a very broad size distribution, and the M_w of these polymers is larger than the M_w of the hydrogenated polymers, while the respective number-averaged molecular weights M_n are smaller.

Typical scattering curves for the small d-PDMAEMA$_{154}$ chains with a narrow size distribution are shown in Figure 2. We find a Guinier plateau starting at $q = 2 \times 10^{-2}$ Å^{-1} and extending to lower q, in agreement with an expected radius of gyration R_g of 5 nm. However, at lower q-values, $q < 5 \times 10^{-3}$ Å^{-1}, the scattered intensity rises sharply again with decreasing q for all salt concentrations. This upturn cannot originate from the tracer molecules, which have a much smaller radius of gyration, but it must originate from the background matrix, which is not perfectly matched to the solvent. We find similar low q upturns in all scattering curves, with an onset point and a scaling that seems independent of salt concentration, polymer chain length and fraction of deuterated chains. We will discuss the origin of this phenomenon in more detail hereafter.

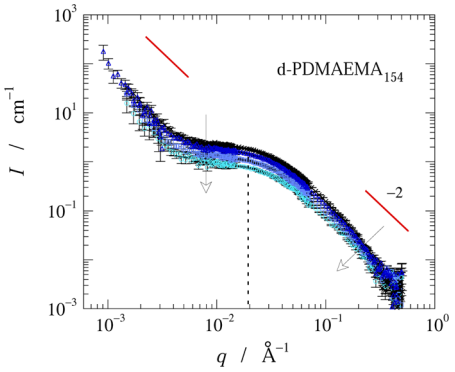

Figure 2. Small angle neutron scattering curves of d-PDMAEMA$_{154}$ tracers (10%) in complex coacervates of h-PAA$_{160}$ and h-PDMAEMA$_{156}$ at different salt concentrations, increasing in the direction of the arrow: 0.80, 0.90, 1.0, 1.1 M KCl. The solid lines indicate a power law slope of −2.

In order to extract the static structure factor of single polymer chains in complex coacervates, we subtracted two scattering curves with different fractions of deuterated tracers (i.e., 10% and 3.3%). As the low q upturn does not originate from the tracer molecules, it is the same in both curves and these contributions cancel out. We have included the raw scattering profiles as separate figures in the Supporting Information. From the resulting subtracted scattering profile we obtain the form factor of a single polymer chain:[33,37]

$$P(q) = \frac{1}{N_b^2}\sum_{n=1}^{N_b}\sum_{m=1}^{N_b}\langle \exp(iq(\vec{r}_n - \vec{r}_m))\rangle$$
$$= \alpha x^{-\alpha}[\gamma(\alpha, x) - x^{\alpha/2}\gamma(\alpha/2, x)]$$
$$\text{with } x = (2\nu + 1)(2\nu + 2)q^2b^2N_b^{2\nu}/6,$$
$$\alpha = 1/\nu, \text{ and } \gamma(s, x) = \int_0^x t^{s-1}e^{-t}dt \quad (1)$$

where b is the Kuhn length, N_b is the number of Kuhn monomers and $\gamma(s,x)$ is the lower incomplete Gamma function, as defined above ($\gamma(s, \infty) = \Gamma(s)$). The shape of the form factor depends on the solvent quality, expressed by ν, the Flory excluded volume parameter ($\nu = 0.5$ for Θ solvents and $\nu = 0.588$ for good solvents). For $1/R_g < q < 1/b$, $P(q) \propto (qb)^{-1/\nu}$ and for $q \ll 1/R_g$, $P(q) \approx (1 - q^2R_g^2/3)$. For Θ solvents, the above equation simplifies to the Debye function for a Gaussian chain: $P(q) = 2[\exp(-q^2R_g^2) - 1 + q^2R_g^2]/q^4R_g^4$.[37,38]

Figure 3 shows the single chain form factors for all deuterated polymers in their corresponding complex coacervates, obtained from the scattering difference of samples with 3.3% and 10% tracers. The scattering from the same deuterated chains in dilute aqueous solution at high salt concentration (1.0−1.2 M) is shown in the same plots for comparison. For

dx.doi.org/10.1021/ma400132s | Macromolecules 2013, 46, 4596−4605

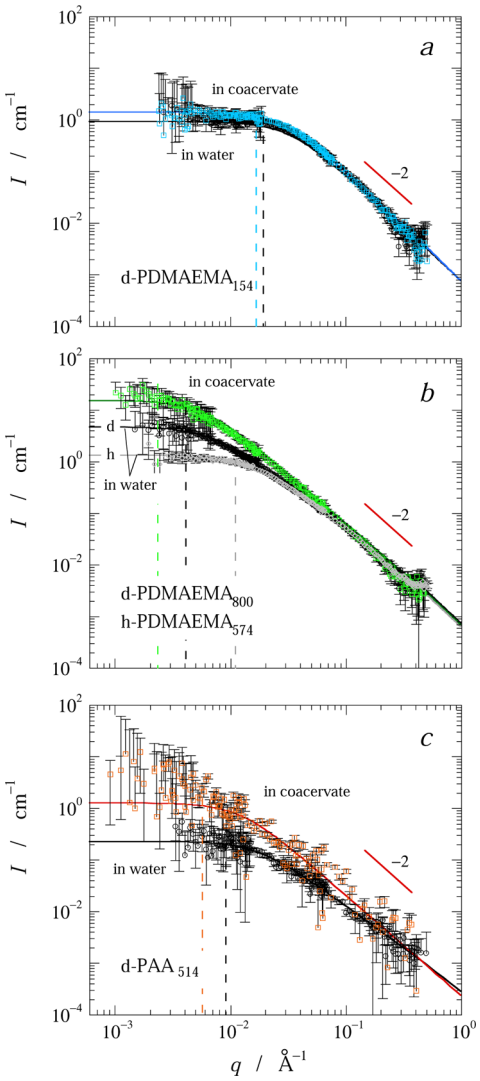

Figure 3. SANS curves of (a) d-PDMAEMA$_{154}$ tracers in solution in H_2O and in complex coacervates of h-PDMAEMA$_{156}$/h-PAA$_{160}$ both at 1.0 M salt; (b) d-PDMAEMA$_{800}$ tracers in solution in H_2O (labeled d), h-PDMAEMA$_{574}$ tracers in solution in D_2O (labeled h), and d-PDMAEMA$_{800}$ tracers in complex coacervates of h-PDMAEMA$_{574}$/h-PAA$_{550}$, all at 1.2 M KCl and (c) PAA$_{514}$ tracers in solution in H_2O and in complex coacervates of h-PDMAEMA$_{574}$/h-PAA$_{550}$ both at 1.2 M KCl. In all cases, the SANS curves in coacervates are the difference curves from the original SANS curves of 3.3% and 10% tracers. The SANS curves in aqueous solution (H_2O and D_2O) are all measured at a tracer amount of 3.3%. The solid lines are fits to eq 1. The dashed lines indicate the inverse radius of gyration ($1/R_g$) of the polymers in aqueous solution and in the complex coacervates.

dilute solutions we never find a low q upturn, as expected. We fitted both curves using the above expression for the form factor of a generalized flexible polymer coil. The fit parameters are summarized in Table 2

In the complex coacervates the polyelectrolytes have a conformation very close to the ideal Gaussian conformation. In aqueous solutions, when the polyelectrolytes are not complexed with oppositely charged polymers, the scaling exponent ν is significantly larger than in the complex coacervates. A few notes should be made together with this general conclusion.

First, the excluded volume parameter for d-PAA in aqueous solutions is slightly higher than the expected $\nu \approx 0.588$ for a hydrophilic, flexible polymer chain in water (good solvent). We believe this is partly caused by the low average scattering intensity we measured for these d-PAA polymers, both in dilute solutions and in complex coacervates, which makes an accurate fit of the slope troublesome. In all samples with d-PAA, the total scattering intensity is roughly an order of magnitude lower than for d-PDMAEMA$_{800}$, despite the fact that the expected scattering length density of d-PAA is quite high (see Table 1). Two possible reasons that can explain this discrepancy are an incomplete deuteration of the d-PAA (verified by H NMR: 10% nondeuterated) and the fact that we typically measure the scattered intensity at very high salt concentrations. Indeed, the scattering length density of the respective salts of d-PAA are lower than the scattering length density in Table 1 (see Supporting Information).[29] Most likely, a combination of both causes the unexpected low scattering intensity from d-PAA samples. Moreover, in dilute solutions the concentration of d-PAA was relatively low and consequently, the error in the detected intensity is large.

Second, the short d-PDMAEMA$_{154}$ are slightly collapsed in the complex coacervates ($\nu < 0.5$), which we attribute to the fact that the initiator used in the synthesis of this polymer is more hydrophobic than for the other polymers, rendering the final polymer less hydrophilic (see also Figure 4a). After complexation with oppositely charged polymers in the complex coacervates, this leads to an effective $\nu < 0.5$.

These experiments show that flexible polymer chains inside complex coacervates are neither much more stiff than in dilute solution, which would be found if oppositely charged chains would form strong parallel chain pairs, corresponding to the "ladder" model for polyelectrolyte complexation,[40] nor fully collapsed into globules. Instead, both types of polymers have a similar conformation, close to the ideal chain conformation that is found for polymers in a melt. Note that, unlike polymer melts, these complex coacervates do still contain large amounts of hydration water and monovalent salt ions.

In contrast to the findings for the swelling parameter ν, the radius of gyration R_g seems to be larger for the polymers in complex coacervates than in dilute solution, although they are less swollen on length scales between the Kuhn length b (of the order of order 2 nm[41,42]) and the radius of gyration R_g. Note that we have not found any region with a different slope (close to q^{-1}) that could indicate a rod-like conformation. Nevertheless, the formation of ionic bonds between the oppositely charged polyelectrolytes could make the polymer chains slightly less flexible,[43] which is translated into a larger Kuhn length b. As a result, the chains will be slightly more stiff than when they are uncomplexed in dilute solution, and their radius of gyration is larger.

Alternatively, the larger radius of gyration might originate from a selection mechanism during the formation of the complex coacervates: mixtures of short chains are more soluble at a given salt concentration than mixtures of long chains, as the saturation concentration of short chains in the dilute phase is higher than that of long chains.[4] When two polymer solutions that both contain a range of sizes are mixed together, the longer chains will preferentially end up in the complex coacervate phases, whereas the shorter chains preferentially end up in the dilute phases. As a result, the complex coacervate contains on average longer polymer chains than the original stock solution. This effect is expected to be more pronounced for polymers with a wider size distribution, such as d-PDMAEMA$_{800}$. Most probably, a combination of both effects, that is, a slight

dx.doi.org/10.1021/ma400132s | Macromolecules 2013, 46, 4596−4605

Table 2. Fit Parameters of the Form Factor of Single Polyelectrolyte Chains in Solution and in Complex Coacervates

polymer	environment	salt concentration (M)	I_0	ν	R_g (nm)	b (nm)[a]
d-PDMAEMA$_{154}$	water	1.0	0.645	0.510	4.62	
	complex coacervate	1.0	1.36	0.460	4.76	3.5
h-PDMAEMA$_{574}$	water	1.2	1.24	0.565	8.31	
d-PDMAEMA$_{800}$	water	1.2	3.47	0.564	15.3	
	complex coacervate	1.2	10.2	0.509	23.5	16
d-PAA$_{514}$	water	1.2	0.232	0.612	7.81	
	complex coacervate	1.2	1.28	0.514	11.7	6.3

[a]Assuming Gaussian statistics: $\langle R_g^2 \rangle = \langle R^2 \rangle/6 \approx N_b b^2/6$. The contour length is calculated from $L = N_b b = Nl$, with l the size of a methacrylate monomer along the contour of the chain, which is assumed to be 0.252 nm,[39] and N the weight-averaged number of methacrylate monomers (see Table 1). The possible selective uptake of long chains in the complex coacervates has not been taken into account, hence, the actual Kuhn are probably smaller.

stiffening and a chain length selection mechanism, underlies the observed larger radius of gyration in Figure 3.

Finally, we note that the conformation hardly depends on salt concentration, in the range we examined (0.8 M < c_s < 1.3 M), as can be seen already in Figure 2.

Structure of Complex Coacervate Networks. In a second series of measurements, we prepared complex coacervates in which all polymers of one type are deuterated and the neutron scattering length density of the solvent is matched to the neutron scattering length density of the other polymer type. This approach allows us to investigate the properties of the network of overlapping polymer chains for both types of chains independently.

We first focus on the scattering profile beyond the low q upturn. We find that the normalized forward scattering of the deuterated networks in the Guinier region is lower than for single polymer chains (see Figure 4). Furthermore, the curves start deviating from the $q^{-1/\nu}$ self-avoiding walk scaling already at higher q, that is, at length scales smaller than the radius of gyration. This implies that the polymer chains overlap in the complex coacervate, like ordinary polymers in a semidilute solution. We determine the correlation length ξ experimentally from the static structure factor of a semidilute polymer solution, which is given by

$$S(q) = \frac{S(0)}{1 + q^2\xi^2} \tag{2}$$

In other words, the structure factor follows a so-called Ornstein−Zernike law, which arises from the modified monomer correlation function in semidilute polymer solutions.[44] The typical correlation length, or mesh size ξ, of the complex coacervates is a few nanometers (see Table 3), which is indeed smaller than the radius of gyration of the polyelectrolytes, indicating that the polymer chains overlap ($\phi > \phi^*$). We find similar mesh sizes for the polycations and the polyanions. The mesh size decreases with decreasing salt concentration, because these complex coacervates are formed by associative phase separation, and the binodal polymer concentration in the complex coacervate phase is higher at lower salt concentrations.[4] The mesh sizes we find experimentally agree well with predictions based on the experimental binodal compositions of these polyelectrolyte complex coacervates[4] and scale as[45]

$$\xi = R_g(\phi^*/\phi)^{m_\xi} \tag{3}$$

where $m_\xi = 1$ in Θ solvents and 3/4 in good solvents. Figure 5 shows the experimental mesh sizes and the prediction based the phase diagram reported in ref 4, using a scaling exponent m_ξ = 1, in agreement with the Gaussian conformations we found above.

In the complex coacervates of the small d-PDMAEMA$_{154}$ we observe an additional apparent structure peak around $q = 3 \times 10^{-2}$ Å^{-1}, which the Ornstein−Zernike law cannot capture (see Supporting Information). We find the same structure peak in these complex coacervates measured with SAXS (see Figure 6a and the discussion there). We note that similar structure peaks in salt-free polyelectrolyte solutions have been ascribed to a characteristic correlation length due to mutual repulsion between the chains.[46] However, such structures typically disappear at very low salt concentration (of order mM). Our samples all have been prepared at quite high salt concentrations and we thus do not expect the structural peak to have the same origin as the structure peak in salt-free polyelectrolyte solutions.

Instead, an alternative explanation can be found from additional interactions between the PDMAEMA chains. It has been found that short PDMAEMA polymers can form micellar structures in water at sufficiently high salt concentrations, due to the hydrophobic initiator groups that are attached to one side of the polymer chains.[47] To model these micelles, we add a second contribution to the total scattering intensity, in which we approximate the micelles as hard spheres with a fixed radius R_m and a volume fraction ϕ_m (see Supporting Information for details on the coupling of structure factors). This model is able to describe the scattering data accurately, as shown in Figure 4a. We find that the size and size distribution of the micelles is only weakly dependent on salt concentration and that the volume fraction increases in the same way as the total polymer concentration with decreasing salt concentration (see Table 3).

In the complex coacervates of d-PAA$_{514}$, the total scattering intensity is again roughly an order of magnitude lower than for the d-PDMAEMA$_{800}$ samples, similar to our findings for d-PAA$_{514}$ in dilute solutions and in the tracer experiments (see Figure 3b). We speculated that these d-PAA are not fully deuterated, or that the neutron scattering length density in aqueous solution with high ionic strength differs significantly from the value in Table 1. Nevertheless, we find that these polymers have a typical correlation length in complex coacervates that is similar to the correlation length for the d-PDMAEMA. However, at high q, corresponding to a typical length scale of 0.3 nm, we find a deviation from the expected scaling of the scattering intensity. The length scale associated with this excess scattering is independent of salt concentration, but it becomes more pronounced at low salt concentrations. This length scale is typical for the size of the chemical monomers and for the average distance between oppositely charged monomers in ionic bonds. We note that some of the

dx.doi.org/10.1021/ma400132s | Macromolecules 2013, 46, 4596−4605

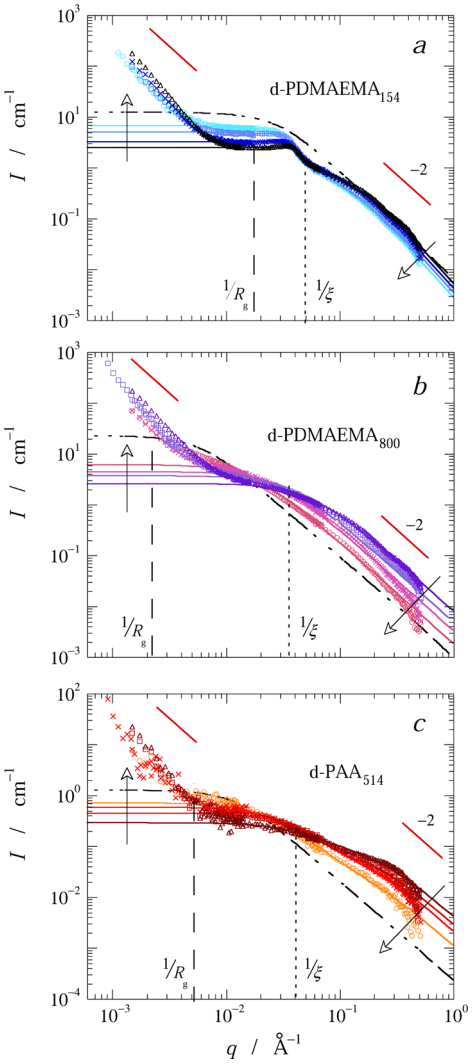

Figure 4. (a) SANS curves of complex coacervates of d-PDMAEMA$_{154}$/h-PAA$_{160}$ with a solvent scattering length density matched to that of h-PAA, at 0.80, 0.90, 1.0, and 1.1 M salt (in the direction of the arrow). The solid lines are model fits to eq 2, combined with a contribution of micelles, which are modeled using a hard-sphere structure factor. (b) SANS curves of complex coacervates of d-PDMAEMA$_{800}$/h-PAA$_{550}$ with a solvent scattering length density matched to that of h-PAA, at 1.0, 1.1, 1.2, and 1.3 M salt (in the direction of the arrow). The solid lines are model fits to eq 2. (c) SANS curves of complex coacervates of h-PDMAEMA$_{574}$/d-PAA$_{514}$ with a solvent scattering length density matched to that of h-PDMAEMA, at 0.90, 1.0, 1.1, and 1.2 M salt (in the direction of the arrow). The solid lines are model fits to eq 2. All vertical dashed and dotted lines indicate the corresponding inverse radius of gyration ($1/R_g$) and the inverse mesh size ($1/\xi$), respectively. The dash-dotted lines that run parallel to the data at high q are the form factor fits of single chains in complex coacervates from Figure 3.

scattering curves for d-PDMAEMA$_{154}$ and d-PDMAEMA$_{800}$ in Figure 4a and b seem to exhibit a small deviation from the expected scaling at similar length scales as well, which is most pronounced at low salt concentrations. However, these features are highly obscured for d-PDMAEMA, because of the significantly higher overall scattering intensity. We can think of two possible explanations for this excess scattering, but we emphasize that additional experiments would have to be done to verify these explanations.

Table 3. Fit Parameters of the Small Angle Neutron Scattering Intensity of Deuterated Complex Coacervate Networks

complex coacervate	salt concentration (M)	$S(0)$	ξ (nm)	ϕ_m	R_m (nm)
d-PDMAEMA$_{154}$/h-PAA$_{160}$	0.80	0.820	1.19	0.22	8.0
	0.90	1.24	1.80	0.20	8.7
	1.0	2.00	2.72	0.17	9.2
	1.1	2.44	4.10	0.14	9.7
d-PDMAEMA$_{800}$/h-PAA$_{550}$	1.0	2.43	1.69		
	1.1	3.45	2.39		
	1.2	5.26	3.87		
	1.3	7.71	6.73		
d-PAA$_{514}$/h-PDMAEMA$_{574}$	0.90	0.211	1.44		
	1.0	0.379	2.16		
	1.1	0.489	2.68		
	1.2	0.725	4.20		

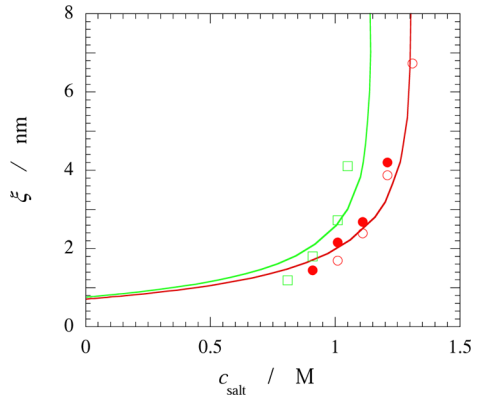

Figure 5. Mesh size of complex coacervates as a function of salt concentration, as determined by SANS. Symbols correspond to d-PDMAEMA$_{800}$/h-PAA$_{550}$ (red ○), d-PAA$_{514}$/h-PDMAEMA$_{574}$ (red ●), and d-PDMAEMA$_{154}$/h-PAA$_{160}$ (green □) complex coacervates. Solid lines are theoretical predictions based on the experimentally determined binodal concentrations of the same polyelectrolyte complex coacervates of $N_{cat} = N_{an} = 150$ and $N_{cat} = N_{an} = 500$.[4] and the scaling law in eq 3.

First, the excess scattering could originate from the ionic bonds between the oppositely charged polyelectrolytes, which occur at a typical distance that corresponds to the q-value of the excess scattering. Although the scattering length density of the solvent was matched to the scattering length density of the oppositely charged hydrogenated polymers in all these complex coacervates, the local scattering length density of the charged groups in an ionic bond may be different from the values reported in Table 1. Since the polymer volume fraction in the complex coacervates and, hence, also the density of ionic bonds, increases with decreasing salt concentration, this contribution to the scattering profile should become more pronounced at low salt concentrations. If, however, the contrast between the deuterated polymer and the solvent is significantly larger than the contribution from the ionic bonds, as is most likely the case for d-PDMAEMA, we expect the contribution from the ionic bonds to the scattering to be obscured.

Alternatively, the initiator groups of one of the polymers, may cause this excess scattering. This length scale would then

dx.doi.org/10.1021/ma400132s | Macromolecules 2013, 46, 4596−4605

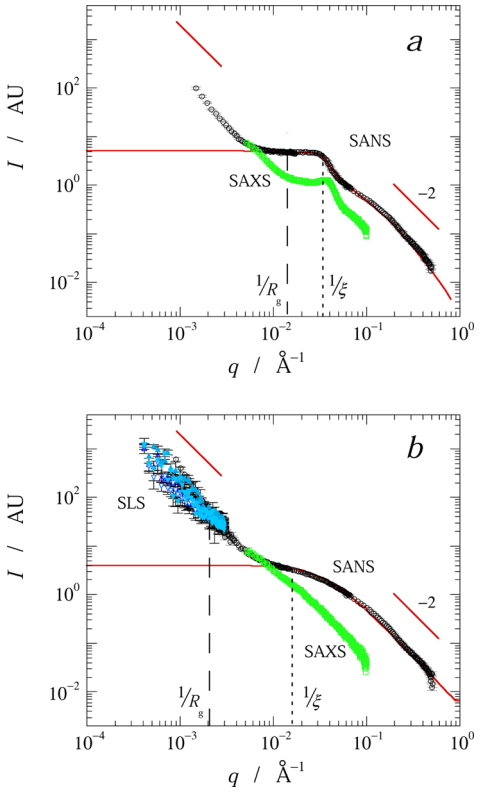

Figure 6. Combination of SANS, SAXS and SLS curves for (a) $PDMAEMA_{156}/PAA_{160}$ and (b) $PDMAEMA_{574}/PAA_{550}$ complex coacervates at salt concentrations of 1.0 and 1.2 M, respectively. The SANS curves were measured on a sample of d-PDMAEMA and h-PAA (see Table 1), the SAXS and SLS curves were both measured on samples of h-PDMAEMA and h-PAA. The solid line is a fit of the SANS data, as in Figure 4. The labels $1/R_g$ and $1/\xi$ indicate the approximate inverse radius of gyration and inverse mesh size of the polyelectrolytes and complex coacervates, respectively.

correspond to the typical size of the initiator moieties, which have a local neutron scattering length density that is different from the (deuterated) polymer backbone. Since the average polymer volume fraction increases with decreasing salt concentration, the concentration of initiator groups also increases with decreasing salt concentration, and the scattering from these groups should become more pronounced at low salt concentration.

Small Angle X-ray and Static Light Scattering. We have complemented our findings on the structure of complex coacervates by SAXS and SLS measurements. In Figure 6, we show our SANS results together with results from SAXS and SLS on the same complex coacervate samples. We have shifted the curves along the vertical axis to overlap in the low q region. We note that the SANS, SAXS and SLS curves show similar characteristics, but they do not overlap completely. In part, this can be explained by the fact that the SANS measurements were carried out for complex coacervates in which all polymer chains of one type were deuterated and the scattering length density of the solvent was matched to that of the oppositely charged polymer, whereas we did not adjust the scattering length densities of the individual components in SAXS and SLS measurements. At the same time, neutrons, X-rays and light interact quite differently with matter: neutrons are scattered by interactions with atomic nuclei, whereas X-rays and light are mainly scattered by interactions with electrons. This leads to a varying relative contrast between the different techniques.[48,49]

Nevertheless, we clearly find that the low q increase in scattering intensity persists in all three techniques. The scattering at low q seems to follow a power law with a slope close to −2 and extend far beyond the radius of gyration of the polymers, indicating that density fluctuations on large length scales are present in the sample. A similar low q upturn in scattering intensity has been observed before in polyelectrolyte gels, semidilute polyelectrolyte solutions,[50] neutral hydrogels,[51] reversible transient gels,[52] and semidilute polystyrene solutions[53,54] and in various protein−polyelectrolyte complex coacervates.[6,24,25] Although the upturn may have different causes in each case, the phenomenon is sometimes referred to as the Picot−Benoît effect, after its first observation.[55]

In protein-polyelectrolyte complex coacervates, the low q scattering has been attributed to the presence of domains of increased density in the complex coacervates, in agreement with observations from cryo-TEM and TIRF.[6,21,22,24,25] To quantitatively describe these scattering curves, the structure factor in eq 2 was combined with a power law, which is also used to model a fractal packing of scatterers.[21,25] In our complex coacervates of flexible polyelectrolytes, we find a similar power law scaling of the scattering intensity at low q with an effective fractal dimension of 2, although no collapsed chains are present that might form a fractal aggregate. We therefore attribute this scattering behavior to the presence of density fluctuations on many length scales, inspired by the observations from cryo-TEM and TIRF.

In our scattering profiles, we find no leveling off of the intensity down to $q = 3 \times 10^{-4}$ Å^{-1}, which would correspond to density fluctuations at length scales up to the micrometer range. Nonetheless, we do not see any inhomogeneities in the complex coacervates with phase contrast microscopy or confocal microscopy on fluorescently labeled polyelectrolytes.[4] We believe that the reason we do not see these density fluctuations with microscopy is the fact that the concentration differences and the differences in refractive index are relatively small. Moreover the fluctuations are probably limited to a few μm, based on the observations by TIRF, which is close to the resolution of optical microscopy.

Finally, we note that a structure peak appears in the small-angle X-ray scattering of $PDMAEMA_{156}/PAA_{160}$ complex coacervates, similar to what we found with SANS. We have attributed this peak to the presence of micelle-like structures, driven by the initiator left over from the synthesis.

Dynamic Light Scattering. Using dynamic light scattering (DLS), we investigated the dynamics of the structures we found with SANS, SAXS and SLS. We used the same complex coacervates as for SANS and SAXS ($PDMAEMA_{574}/PAA_{550}$). We clearly find two dynamic processes occurring, as can be seen in Figure 7. The phase autocorrelation functions can be fitted with the following empirical equation:[56]

$$g_1(t) = A_1 \exp(-(t/\tau_1)^{\alpha}) + A_2 \exp(-(t/\tau_2)^{\beta}) \quad (4)$$

where t is the correlation time, α and β are stretch exponents, τ_i is the relaxation time, and A_i is the amplitude of mode i, with $\sum_i A_i = 1$.

Both processes have a diffusive origin, as the corresponding relaxation times scale with q^{-2} (see Figure 8a). The stretch exponents vary between 0.6 and 1.0 and are independent of q. For the PDMAEMA/PAA complex coacervate, we estimate the

dx.doi.org/10.1021/ma400132s | Macromolecules 2013, 46, 4596−4605

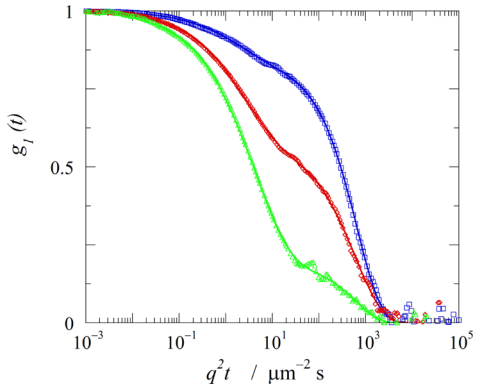

Figure 7. Normalized autocorrelation functions from DLS versus q^2t for h-PDMAEMA$_{574}$/h-PAA$_{550}$ complex coacervates at a salt concentration of 1.2 M, measured using a detector angle of 40°, 68° and 110°, from right to left. We note that a weak oscillation with a period of about 100 ms is visible in the correlation functions, due to a coupling of the cooling elements in the diode laser. These oscillations are not related to relaxation processes in the samples.

typical size related to the diffusive mode from the Stokes–Einstein equation and the measured viscosity of this particular complex coacervate (η = 400 mPa s). We find that the fast mode corresponds to objects of 1–2 nm, that is, comparable to the mesh size of the complex coacervate (see Figure 5). This mode probably results from fluctuations of the overlapping chains, which leads to fluctuations of the mesh size. The slow mode corresponds to diffusion of much larger objects (R = 200 – 500 nm). We believe the slow mode is related to the large-scale density fluctuations we find in static scattering experiments.

CONCLUSIONS

We have carried out small angle neutron scattering on PDMAEMA/PAA complex coacervates. Using deuterated polymeric tracers in a complex coacervate for which we match the neutron scattering length density to that of the solvent, we measure single chain static structure factors of the polycation and the polyanion. Both have an almost Gaussian conformation, both for short and long polymer chains. Clearly, the charge-driven association of the oppositely charged polyelectrolytes does not lead to collapse into globules, nor to stiffening as a result of the formation of hypothetical pairs of parallel polymers (ladder model). Using all deuterated chains of one type in the complex coacervate networks, we find that the complex coacervates are interpenetrated overlapping polymer solutions, similar to semidilute solutions of neutral polymer chains. Combining our SANS results with small-angle X-ray and static light scattering, we find a remarkable excess scattering at low q for all complex coacervates, following a power law scaling with a slope close to −2. We do not find a leveling off down to $q \approx 3 \times 10^{-4}$ Å^{-1}. This scattering is independent of chain length, salt concentration and polymer concentration. We attribute it to large-scale, equilibrium density fluctuations inside the complex coacervates, similar to the findings for protein-polyelectrolyte complex coacervates. In dynamic light scattering we find two diffusive modes of relaxation, in agreement with the static structure: the fast mode corresponds to fluctuations of the mesh size, the slow mode corresponds to diffusion of the domains of varying density.

ASSOCIATED CONTENT

Supporting Information

Scattering length densities of PDMAEMA and PAA, match point of complex coacervate scattering length, tracer experiments, and structure factor of d-PDMAEMA$_{154}$ samples. This material is available free of charge via the Internet at http://pubs.acs.org/.

AUTHOR INFORMATION

Corresponding Author

*E-mail: (J.v.d.G) jasper.vandergucht@wur.nl.

Notes

The authors declare no competing financial interest.

ACKNOWLEDGMENTS

The authors would like to thank Dr. Ilja Voets (TU/e) and Barend van Lagen (WUR) for supplying cuvettes and discussing the results and Dr. Marc Lemmers (Unilever) for his help with the SAXS measurements and fruitful discussions. ES acknowledges The Netherlands Organisation for Scientific Research (NWO) for financial support and for providing beamtime at the Dutch-Belgian Beamline (DUBBLE), BM26.

REFERENCES

(1) van der Gucht, J.; Spruijt, E.; Lemmers, M.; Cohen Stuart, M. A. *J. Colloid Interface Sci.* **2011**, *361*, 407–422.

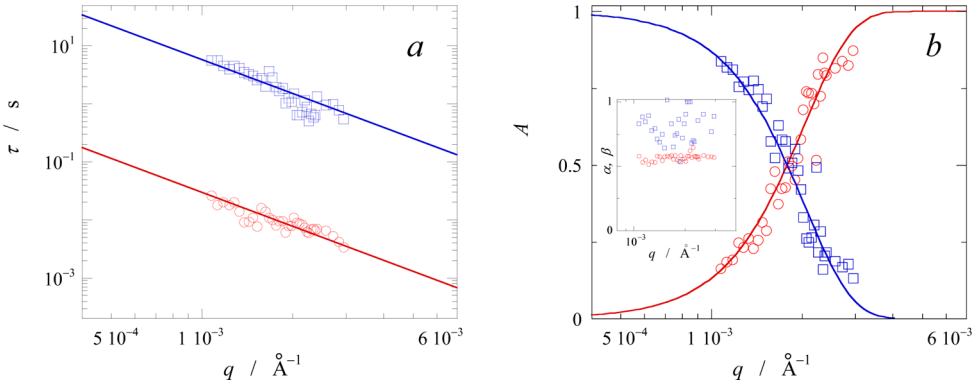

Figure 8. (a) Intensity decay times τ, corresponding to the rate of dynamic relaxation in DLS measurements of h-PDMAEMA$_{574}$/h-PAA$_{550}$ at 1.2 M salt, as a function of q. The solid line indicates a power law with a slope of −2. (b) Amplitudes corresponding to the decay times in part a as a function of q. The solid lines are drawn to guide the eye. The inset shows the corresponding stretch factors α and β from eq 4.

(2) de Kruif, C. G.; Weinbreck, F.; de Vries, R. *Curr. Opin. Colloid Interface Sci.* **2004**, *9*, 340−349.
(3) Bungenberg-de Jong, H. G.; Kruyt, H. R. *Proc. KNAW* **1929**, *32*, 849−856.
(4) Spruijt, E.; Westphal, A. H.; Borst, J. W.; Cohen Stuart, M. A.; van der Gucht, J. *Macromolecules* **2010**, *43*, 6476−6484.
(5) Spruijt, E.; Sprakel, J.; Lemmers, M.; Cohen Stuart, M. A.; van der Gucht, J. *Phys. Rev. Lett.* **2010**, *105*, 208301.
(6) Kizilay, E.; Kayitmazer, A. B.; Dubin, P. L. *Adv. Colloid Interface Sci.* **2011**, *167*, 24−37.
(7) Stewart, R. J.; Wang, C. S.; Shao, H. *Adv. Colloid Interface Sci.* **2011**, *167*, 85−93.
(8) Overbeek, J. T. G.; Voorn, M. J. *J. Cell. Comp. Phys.* **1957**, *49*, 7−26.
(9) de Vries, R. *Biochimie* **2010**, *92*, 1715−1721.
(10) Clark, D. J.; Kimura, T. *J. Mol. Biol.* **1990**, *211*, 883−896.
(11) Widom, J. *Annu. Rev. Biophys. Biomol. Struct.* **1998**, *27*, 285−327.
(12) Clausell, J.; Happel, N.; Hale, T. K.; Doenecke, D.; Beato, M. *PLoS ONE* **2009**, *4*, e0007243.
(13) Capito, R.; Azevedo, H.; Velichko, Y.; Mata, A.; Stupp, S. *Science* **2008**, *319*, 1812−1816.
(14) Biesheuvel, P. M.; Mauser, T.; Sukhorukov, G. B.; Möhwald, H. *Macromolecules* **2006**, *39*, 8480−8486.
(15) van der Kooij, H. M.; Spruijt, E.; Voets, I. K.; Fokkink, R.; Cohen Stuart, M. A.; van der Gucht, J. *Langmuir* **2012**, *28*, 14180−14191.
(16) Martens, A. A.; van der Gucht, J.; Eggink, G.; de Wolf, F. A.; Cohen Stuart, M. A. *Soft Matter* **2009**, *5*, 4191−4197.
(17) Lemmers, M.; Sprakel, J.; Voets, I.; van der Gucht, J.; Cohen Stuart, M. *Angew. Chem., Int. Ed.* **2010**, *49*, 708−711.
(18) Hone, J. H. E.; Howe, A. M.; Cosgrove, T. *Macromolecules* **2000**, *33*, 1206−1212.
(19) Hone, J. H. E.; Howe, A. M.; Cosgrove, T. *Macromolecules* **2000**, *33*, 1199−1205.
(20) Weinbreck, F.; Rollema, H. S.; Tromp, R. H.; de Kruif, C. G. *Langmuir* **2004**, *20*, 6389−6395.
(21) Kayitmazer, A. B.; Strand, S. P.; Tribet, C.; Jaeger, W.; Dubin, P. L. *Biomacromolecules* **2007**, *8*, 3568−3577.
(22) Bohidar, H.; Dubin, P. L.; Majhi, P. R.; Tribet, C.; Jaeger, W. *Biomacromolecules* **2005**, *6*, 1573−1585.
(23) Wang, X.; Li, Y.; Wang, Y.-W.; Lal, J.; Huang, Q. *J. Phys. Chem. B* **2007**, *111*, 515−520.
(24) Singh, S. S.; Aswal, V. A.; Bohidar, H. B. *Int. J. Biol. Macromol.* **2007**, *41*, 301−307.
(25) Chodankar, S.; Aswal, V. A.; Kohlbrecher, J.; Vavrin, R.; Wagh, A. G. *Phys. Rev. E* **2008**, *78*, 031913.
(26) Glasoe, P. K.; Long, F. A. *J. Phys. Chem.* **1960**, *64*, 188−189.
(27) Rehfeldt, F.; Steitz, R.; Armes, S. A.; von Klitzing, R.; Gast, A. P.; Tanaka, M. *J. Phys. Chem. B* **2006**, *110*, 9177−9182.
(28) Brandrup, J.; Immergut, E. H. *Polymer Handbook*; John Wiley & Sons: 1966.
(29) Berret, J.-F.; Yokota, K.; Morvan, M.; Schweins, R. *J. Phys. Chem. B* **2006**, *110*, 19140−19146 Note: this paper contains a miscalculation, a density of 1.5 leads to the reported SLD of 2.09..
(30) Hourdet, D.; L'Alloret, F.; Durand, A.; Lafuma, F.; Audebert, R.; Cotton, J.-P. *Macromolecules* **1998**, *31*, 5323−5335.
(31) Moglianetti, M.; Li, P.; Malet, F. L. G.; Armes, S. A.; Thomas, R. K.; Titmuss, S. *Langmuir* **2008**, *24*, 12892−12898.
(32) Spruijt, E.; Cohen Stuart, M. A.; van der Gucht, J. *Macromolecules* **2013**, *46*, 1633−1641.
(33) http://kur.web.psi.ch/sans1/sanssoft/sasfit.html.
(34) Lemmers, M.; Spruijt, E.; Beun, L.; Fokkink, R.; Leermakers, F. A. M.; Portale, G.; Cohen Stuart, M. A.; van der Gucht, J. *Soft Matter* **2012**, *8*, 104−117.
(35) Moreels, E.; De Ceuninck, W.; Finsy, R. *J. Chem. Phys.* **1987**, *86*, 618−623.
(36) Wu, H. *Chem. Phys.* **2010**, *367*, 44−47.
(37) Hammouda, B.; Akcasu, A. Z.; Benmouna, M. *J. Polym. Sci. B* **1984**, *22*, 853−862.
(38) Doi, M.; Edwards, S. F. *The theory of polymer dynamics*; Oxford University Press: Oxford, U.K., 1986.
(39) Rathgeber, S.; Pakula, T.; Wilk, A.; Matyjaszewski, K.; Beers, K. *J. Chem. Phys.* **2005**, *122*, 124904.
(40) Lazutin, A. A.; Semenov, A. N.; Vasilevskaya, V. V. *Macromol. Theory Simul.* **2012**, *21*, 328−339.
(41) Walczak, W. J.; Hoagland, D. A.; Hsu, S. L. *Macromolecules* **1992**, *25*, 7317−7323.
(42) Miquelard-Garnier, G.; Creton, C.; Hourdet, D. *Soft Matter* **2008**, *4*, 1011−1023.
(43) Spruijt, E.; van den Berg, S. A.; Cohen Stuart, M. A.; van der Gucht, J. *ACS Nano* **2012**, *6*, 5297−5303.
(44) Lindner, P., Zemb, T., Eds. *Neutrons, X-rays and light: scattering methods applied to soft condensed matter*; Elsevier Science: Amsterdam, 2002.
(45) de Gennes, P. G. *Scaling Concepts in Polymer Physics*; Cornell University Press: Ithaca, NY, 1979.
(46) Norwood, D. P.; Benmouna, M.; Reed, W. F. *Macromolecules* **1996**, *29*, 4293−4304.
(47) Liu, Q.; Yu, Z.; Ni, P. *Colloid Polym. Sci.* **2004**, *282*, 387−393.
(48) Pedersen, J. S. *Adv. Colloid Interface Sci.* **1997**, *70*, 171−210.
(49) Sommer, C.; Pedersen, J. S.; Garamus, V. M. *Langmuir* **2005**, *21*, 2137−2149.
(50) Horkay, F.; Hecht, A.; Geissler, E. *J. Polym. Sci., Part B: Polym. Phys.* **2006**, *44*, 3679−3686.
(51) Lin-Gibson, S.; Jones, R.; Washburn, N.; Horkay, F. *Macromolecules* **2005**, *38*, 2897−2902.
(52) Blanco, M.; Leisner, D.; Vázquez, C.; Lopéz-Quintela, M. *Langmuir* **2000**, *16*, 8585−8594.
(53) Dautzenberg, H. *J. Polym. Sci. C* **1972**, *39*, 123−131.
(54) Koberstein, J.; Picot, C.; Benoit, H. *Polymer* **1985**, *26*, 673−681.
(55) Benoit, H.; Picot, C. *Pure Appl. Chem.* **1966**, 545−561.
(56) Li, J.; Ngai, T.; Wu, C. *Polym. J.* **2010**, *42*, 609−625.